Pectin Conformation in Solution

Journal:	*The Journal of Physical Chemistry*
Manuscript ID	jp-2018-047904.R1
Manuscript Type:	Article
Date Submitted by the Author:	n/a
Complete List of Authors:	Alba, Katerina; University of Huddersfield, Biological Sciences Bingham, Richard; University of Huddersfield, Biological Sciences Gunning, Patrick; Quadram Institute Bioscience Wilde, Peter; Quadram Institute Bioscience Kontogiorgos, Vassilis; University of Huddersfield, Biological Sciences

Pectin Conformation in Solution

K. Alba[a], R. J. Bingham[a], P. A. Gunning[b], P. J. Wilde[b], and V. Kontogiorgos[a*]

[a]Department of Biological Sciences, University of Huddersfield, HD1 3DH, UK

[b]Quadram Institute Bioscience, Norwich Research Park, Norwich, NR4 7UA, UK

*Corresponding author email: v.kontogiorgos@hud.ac.uk

Abstract

The interplay of degree of methylesterification (DM), pH, temperature, and concentration on the macromolecular interactions of pectin in solution has been explored. Small angle X-ray scattering complemented by atomic force microscopy and molecular dynamics were employed to probe chain dimensions and solution structure. Two length scales have been observed with the first characterising chain clustering with a size ranging between 100-200 nm. The second level of structure arises from single biopolymer chains with radius of gyration between ~6-42 nm. The development of a range of macromolecular dimensions *in vitro* and *in silico* shows chain flexibility increases with DM and at acidic pH whereas hydrogen bonding is the responsible thermodynamic driving force for cluster formation. High methyl pectins create structures of lower fractal dimension with less efficient packing. This work unveils pectin conformations covering most of its industrially and biologically relevant environments, enabling rational design of advanced biomaterials based on pectin.

1. Introduction

Research on the solution conformation of biomacromolecules is imperative, as this ultimately controls their functionality either *in vivo* or after appropriate modifications (*e.g.,* purification or functionalisation) their industrial applications. Biological macromolecules are most frequently dispersed in aqueous environments as opposed to synthetic polymers where an organic solvent is most commonly used. Aqueous environments create complications due to the large number of interactions that may occur simultaneously depending on the fine structure of the biopolymer (*e.g.*, hydrogen, hydrophobic, or ionic interactions).[1] Upon dispersion, chains expose their functional groups in the aqueous environment (*e.g.,* methyl, amine, carboxyl etc.) and the interplay between the ensuing macromolecular interactions may be either favourable, resulting in dissolution, or unfavourable resulting in self-association. Tuning of these interactions usually occurs by controlling fine structure of the biopolymer, composition of the aqueous environment (*e.g.,* pH, ionic strength, type of cation, etc.), or temperature as it dictates the conformational state of the biopolymer in solution. This in turn is crucial as it controls the gelation mechanisms, arrangement at the interfaces or has implications in post-harvest biology of crops (*e.g.,* ripening of fruits and vegetables).[2]

The already convoluted landscape of biopolymers becomes even more complex when the macromolecule carries several functional groups, different sugar residues, and has a diverse branching pattern. In these cases, functionality is also determined by the distribution of the functional groups and grafting of the chains. [3] Pectin is a heteropolysaccharide that in its simplest form could be regarded as a di-block copolymer of two major segments. Homogalacturonan (HG) consists of linear (1→4) linked α-D-galacturonic acid (D-GalA) with variable degrees of methyl esterification (DM) of the carboxyl group at the C-6 position and depending on the origin acetyl-esters at O-2 and/or O-3 positions of GalA may also be present. If DM is lower than 50% pectin is classed as low methylated (LM) whereas if it is higher than 50% as high methylated (HM) that brings about substantial ramifications to functionality, as for instance on the gel-formation

mechanism. Rhamnogalacturonan-I (RG-I) is the second major segment consisting of alternating units of rhamnose (Rha) and galacturonic acid [α-(1→2)-D-GalA–α-(1→4)-L-Rha]$_n$ with n being frequently higher than 100. Rhamnose residues frequently carry branches at O-4 and/or O-3 positions of Rha consisting of galactose, arabinose, and in certain pectins, protein moieties are also found.[4] As a result of the polyelectrolyte (carboxyl groups) and hydrophobic (methyl groups) nature of pectin, the location and distribution of methyl and charged groups along the chain (termed blockiness) also controls functionality and is remarkably difficult to assess and industrially reproduce.[5] As a silver lining, the concurrent presence of all the above-mentioned parameters makes pectin a highly tunable polysaccharide for a large number of applications.

A lot of analytical work has been devoted on structure characterisation of pectin but literature on the solution conformation of pectin is sparse particularly with scattering methods. Previous work has identified that pectins rich in HG domains are semi flexible macromolecules[6] and as RG-I domains increase the chains acquire greater conformational freedom due to the flexibility that is imparted by the presence of rhamnose.[7] In addition, measurable conformational changes seem to occur only when pH is raised above ~4, which is related to the dissociation constant of galacturonic acid (pK_a 3.5 at 20 ^oC).[8] However, chain conformation in solution is not only related to the structure of the biopolymer but is also inherently associated with the thermodynamic properties of the aqueous solvent. Crucially, the interplay between molecular interactions that control pectin conformation and therefore functionality, as affected by both pectin structure and solvent quality is not well understood. The objectives of the present work were, therefore, to bridge this gap of understanding by investigating the influence of key structural parameters (degree of methylesterification), solvent quality (pH, temperature, salt) and concentration in an effort to present detailed relationships of the spatial arrangements of pectin for essentially most of its biologically and industrially relevant conditions.

2. Materials and Methods

2.1 Materials

Two samples of pectin (CP-Kelco, UK) with degree of methylesterification (DM) 7% and 75% have been used in the present investigation. Samples were washed in 60% ethanol to remove any residual monosaccharides that may interfere with background subtraction in SAXS measurements and freeze-dried. The two freeze-dried samples (DM 7 and 75) were then mixed in order to obtain pectin samples with degree of methylesterification 10, 30, 50, and 70 % labelled as DM 10, DM 30, DM 50 and DM 70, respectively. Sodium chloride, potassium chloride and 3-(N-morpholino)propanesulfonic acid (MOPS) were obtained from Sigma Aldrich (Poole, UK).

2.2 Sample preparation

Samples were dispersed at 1, 3 or 10 mg/mL in 100 mM buffers at either pH 1.0 (HCl/KCl) or 7.0 (MOPS) in the presence or absence of 100 mM NaCl. Samples were left overnight under continuous stirring to ensure complete solubilisation. Following solubilisation, samples were centrifuged to remove any insoluble material or aggregates and were subjected to SAXS measurements at 10, 30, 50 or 65 ^{o}C, as described below.

2.3 Molecular characterisation of samples

The weight- and number-average molecular weights (M_w, M_n), polydispersity index, and radius of gyration of the samples were estimated using size exclusion chromatography coupled to multi-angle laser light scattering (SEC-MALS) at 25 ^{o}C. Pectins were solubilised in 100 mM $NaNO_3$ solution (3 mg mL^{-1}) at ambient room temperature with stirring overnight. Samples were subsequently injected onto a SEC system (15 mm particle size, 25 cm, 4 mm, Agilent, Oxford, UK) which consisted of a PL Aquagel guard column linked in series with PL Aquagel-OH 60, PL Aquagel-OH 50, and PL Aquagel-OH 40. Pectins were eluted with 100 mM $NaNO_3$ solution (pH 8.6) at a flow rate of 0.7 mL min^{-1}. The eluent was then detected online firstly by a DAWN EOS light scattering detector (Wyatt Technology, Santa Barbara, U.S.A.) followed by a rEX

differential refractometer (Wyatt Technology, Santa Barbara, U.S.A.). The refractive index increment, dn/dc was taken to be 0.146 mL g^{-1}. [9] Intrinsic viscosity ([η]) measurements on pectins were performed using an Ubbelohde capillary viscometer after dispersion at 0.01-1 gdL^{-1} in buffers with 100 mM NaCl at pH 1.0 or 7.0 at 20 ^{o}C. Determination of the intrinsic viscosities for each of the different pectin extracts were obtained by extrapolation to infinite dilution using the Huggins relationship.[10] Fourier transform infrared (FTIR) analysis was used to calculate the degree of methylesterification of samples after constructing a calibration curve using commercial pectins with known degree of methylesterification.[11] FTIR spectra were obtained between 500 and 4000 cm^{-1} for all samples in attenuated total reflection (ATR) mode at a resolution of 4 cm^{-1} using 128 scans (Nicolet 380, Thermo Scientific, UK). Spectral smoothing was applied using instrument software (OMNIC 3.1). Protein quantification was performed using Bradford assay. [12]

2.4 SAXS measurements and data analysis

Small angle X-ray scattering (SAXS) experiments were performed at B21 of the Diamond Light Source (Didcot, Oxford, UK) in batch mode using the bioSAXS sample delivery robot (Arinax, Grenoble France). 30 µL samples were arrayed in a 96-well plate and loaded into a 1.5 mm internal diameter, 10 µm thick quartz capillary sample cell. Sample cells were maintained at temperatures of 10, 30, 50 and 65 ^{o}C where indicated. For each sample, total exposure time was 180 sec taken as an exposure set of 60 x 3 sec frames. SAXS measurements were performed at 12.4 keV using a fixed 4 m camera length and a Dectris Pilatus 2M detector. Images were scaled, integrated and reduced to a 1D SAXS curve using the DAWN. [13] The instrument was calibrated using the powder diffraction rings of silver behenate. Radiation induced changes was assessed by noting changes in the SAXS curves over the frame set. Buffer or background subtraction was performed using an in-house processing pipeline and Scatter (v3.0, www.bioisis.net). Briefly, measurements corresponding to buffer were averaged and subtracted from each frame within sample exposure set. Subtracted frames that were considered identical were averaged to produce a single, merged SAXS curve representing the sample. Data analysis was performed using both

Scatter (v3.0, www.bioisis.net) and SasView (v4.1.1, www.sasview.org). Scatter was used to obtain, the cross-sectional radius of gyration (R_c) that was calculated using the Guinier approximation from the intermediate q-region so as $q \times R_c < 1.4$. Kratky plots were constructed to examine the conformational changes of pectin and double logarithmic intensity plots to obtain the fractal exponents by fitting a power law function. A two-correlation length model was fitted to the data to obtain correlation length, ξ using SasView.

2.5 Atomic Force Microscopy imaging

The pectin solutions were diluted to 2 μg mL^{-1} in ultrapure H_2O (18.2 MΩ) and then 2 μL drop deposited onto freshly cleaved mica and fully evaporated in 20 mins at room temperature (~20 ◦C). The AFM used for the present studies was manufactured by ECS (East Coast Scientific, Cambridge, UK). Contact (repulsive force) imaging was carried out under constant force conditions (1 nN). The AFM probes used were short Silicon Nitride cantilevers (Budget Sensors, Innovative Solutions Bulgaria Ltd., Sofia, Bulgaria) with a quoted force constant of 0.27 N m^{-1}.

2.6 Molecular Dynamics

Molecular dynamics (MD) simulations were conducted using the AmberTools17 suite of software[14] and the GLYCAM06j parameters for carbohydrates.[15] Decamers of 1→4-linked α-D-GalA with either methyl-esterification or protonation at the C-6 position were built in *xleap* and *tleap* and neutralized by the addition of sodium ions. Additional Na^+ and Cl^- ions were added to maintain an equal ionic strength (~100 mM) in all conditions. The system was then solvated in explicit water using a periodic cubic box with a minimum contact distance of 8 Å and the TIP3P water model. After energy minimisation, the system was heated at constant volume (boundary condition flag ntb = 1, pressure regulation flag ntp = 0) from 0 to 300 ^oK before an equilibration step at constant pressure (1 bar) with isotropic position scaling (ntp = 1, ntb = 2). Molecular dynamics production runs continued under constant pressure with a relaxation time of 2 ps. Bond lengths involving hydrogen were constrained with the SHAKE algorithm (bond length constraint

flag ntc = 2). Four systems were simulated, DM10 at pH 1 and pH 7, and DM70 at pH 1 and pH 7. It was assumed that all carboxylic acid groups were either fully protonated or fully deprotonated at pH 1 and 7, respectively. CPPTRAJ[16] was used to process MD trajectory files (strip waters) and calculate dihedral angles from the last 6 ns of each 10 ns simulation. φ and ψ dihedral angles were defined as: φ = O-5 C-1 O-1 C-4′ and ψ = C-1 O-1 C-4′ C-5′. Contour plots to show the distribution of φ/ψ angles over all nine bonds in the decamer over the last 6 ns of simulation (54,000 data points) were generated in R.[17] Decamer chain lengths were calculated in the Visual Molecular Dynamics software.[18] Figures of representative pectin oligomers were generated in PyMOL.[19]

3. Results and Discussion

3.1 Sample characterisation and qualitative examination of scattering curves

Samples used for SAXS measurements were characterised for molecular attributes relevant to the present investigation. As all samples were formed by mixing two commercial pectin powders, the actual degree of methylesterification was determined and it was found to be very close to the expected values (Table 1).

Table 1: Molecular characteristics of pectins that were used in the present investigation. R_g has been obtained from SEC-MALS measurements.

	DM 10	**DM 30**	**DM 50**	**DM 70**
$M_w \times 10^3$ (g mol^{-1})	276	273	199	197
$M_n \times 10^3$ (g mol^{-1})	105	133	108	111
R_g (nm)	35	33	36	36
M_w/M_n	2.6	2.1	1.8	1.8
Protein (% w/w d.b.)	0.19 ±0.10	0.07 ±0.02	0.90 ±0.02	0.36 ±0.10
Measured DM (%)	13 ±0.2	26 ±0.4	52 ±0.6	72 ±0.8
[η] dLg^{-1} at pH 1	0.3	1.4	3.3	4.7
[η] dLg^{-1} at pH 7	0.7	2.1	3.9	5.3

Commercial pectins are already a mixture of chains differing in the distribution of both charges and methyl groups.[20, 21] On a molecular level, the original samples will also have a distribution of DM in the pectin chains present *i.e.,* not all the individual macromolecules will have the same DM. As a result, the present approach yields samples not only with a gradual transition in the DM but also in the degree of blockiness albeit the latter was not quantified in the present work. Furthermore, powder mixing removes an additional level of complexity, which is associated with molecular weight distribution, as is discussed below. Cross contamination from protein that naturally occurs in commercial pectin preparations was found to be negligible, and consequently, protein will not have measurable contribution to the scattering patterns of pectin solutions. Weight-average molecular weight (M_w) of samples with DM 10 and 30 were slightly higher than those with DM 50 and 70 due to size differences in the initial materials that were used to create the samples. However, number-average molecular weight (M_n) that emphasizes the presence of macromolecules with low molecular size and the radius of gyration (R_g) are comparable between the samples. As a result, most of scattering particles have similar size affording valid comparisons to be made between the samples. Intrinsic viscosity ([η]) was also estimated in the presence of salt at the same pH values as with the SAXS measurements. Generally, intrinsic viscosity was higher at pH 7 reflecting the expansion of the coils due to dissociation of galacturonic acid. In addition, [η] increases with DM an observation that is also reflected in the lower fractal dimensions of high-DM pectin samples (i.e., less efficient packing of the chains resulting in greater volume occupancy), as it will be shown later.

SAXS traces of pectin samples were obtained in the presence or absence of salt but only the former results are presented and discussed. High salt concentration (100 mM) is essential to minimise conformational changes due to intra- and inter-molecular Coulombic interactions.[22] Consequently, scattering is expected to originate from chain conformations with minimal contribution from Coulombic interactions. Scattering intensity curves are characterised by two

dominant features that represent two different length scales in the solution structure of the samples (Figure 1).

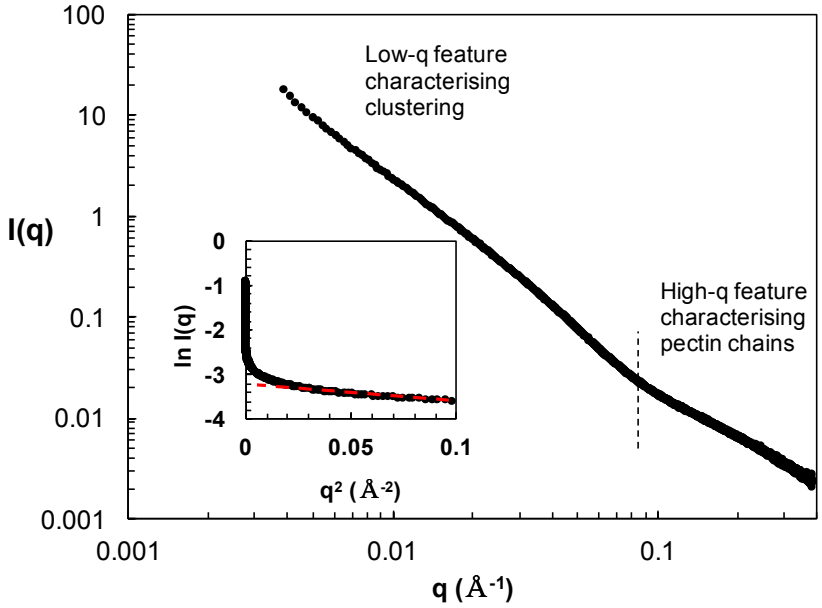

Figure 1: Typical small-angle X-ray scattering intensity plot of pectin samples exhibiting two distinct length scales. Inset shows the region that was taken to calculate the cross-sectional radius of gyration (R_c) ($q > \sim 0.1$ Å).

The low-q region ($q < \sim 0.1$ Å^{-1}) characterises large size clusters whereas the high-q regime ($q > \sim 0.1$ Å^{-1}) arises from the scattering of the biopolymer chains. The asymptotic growth of the scattering curve along y-axis is common in SAXS from polysaccharide solutions (*e.g.,* alginates,[23] carragennan,[24] or bacterial polysaccharides[25]) or hydrophilic synthetic polymers[26] in contrast to pristine monodispersed protein solutions where the Guinier regime is normally observed. Cluster sizes are greater than the resolution of the present technique and therefore their dimensions cannot be probed. Concentration dependence experiments and concentration-normalised scattering plots did not reveal any changes in the shapes of the curves showing that no new structures are formed in the semi dilute region of the polymers (Figure S1). Initial qualitative evaluation of the influence

of the studied parameters on chain disorder is achieved by Kratky plot construction (q^2I(q) *vs.* q, Figure 2).

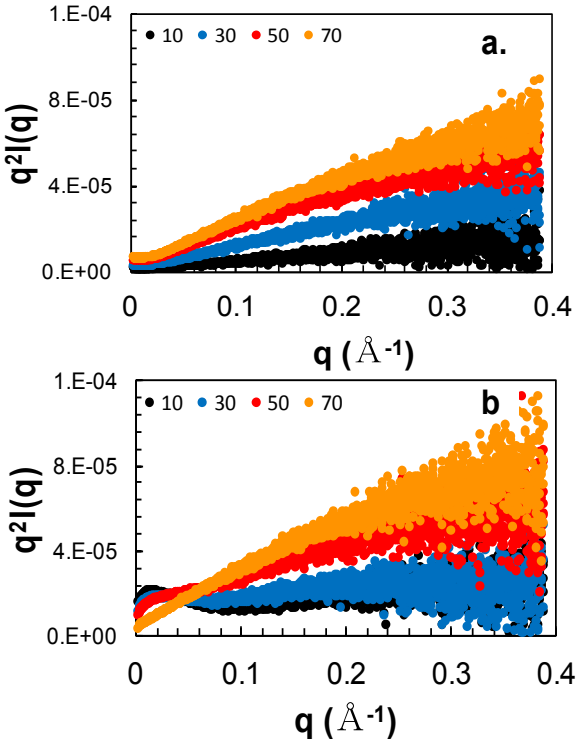

Figure 2: Typical Kratky plots of pectin samples with different DM at (a) pH 1, and (b) pH 7. Curves increase monotonically at pH 1 indicating extended conformation. A peak that appears at pH 7 at around 0.015 Å^{-1} and gradually disappears with increase of DM is a result of counterion condensation.

The curves of all samples at pH 1 increase monotonically, indicating disordered chains at all conditions studied (Figure 2a). At pH 7 a peak that emerges in the low-q region at about 0.015 Å^{-1} indicates that chains attain a more folded conformation that gradually disappears with increase of DM (Figure 2b). This behaviour is attributed to counterion condensation effect that forces chains into a more coiled conformation.[27-29] In the presence of added salt (usually above a certain salt concentration) pectin forms complexes between positively charged sodium and negatively charged carboxylic acids, which is facilitated at pH 7 due to deprotonation of carboxylic acid. At higher DM the peak decreases in intensity and ultimately disappears at DM 70 where charge density

decreases[30] and methylesterification of carboxylic acids minimizes the influence of counterion condensation. This is further supported by Kratky plots obtained for salt-free samples where the peak at 0.015 $Å^{-1}$ is not observed (Figure S2) and from intrinsic viscosity measurements where, as discussed previously, the chains occupy greater hydrodynamic volume at high pH values (Table 1). Similar behaviour of chain conformations in polyelectrolyte systems has been previously experimentally observed, [31, 32] theoretically predicted, [29] or simulated in molecular dynamics.[33, 34]

3.2 Quantitative analysis of SAXS curves

SAXS-curve analysis permits following characteristic sizes with changes in solvent thermodynamics (pH and temperature) and pectin molecular architecture (DM) to achieve a quantitative examination of chain dimensions. Absence of Guinier regime due to the characteristic aggregation does not allow calculation the radius of gyration of the clusters ($R_{cluster}$). However, the radius of gyration of the cross-section (R_c) was calculated from the high-q region of the curves (Figure 1, inset) for all samples and was found to range between about 3-7 Å (Table S1) with samples at pH 7 showing a tendency to have greater R_c with a difference of about 2 Å. The effect was more prominent for samples with low DM whereas with increase of the methyl content in the samples the influence of pH subsides. Higher R_c values of low DM pectins is due to local chain bending due to counterion condensation in agreement with Kratky plots (Figure 2b) and molecular dynamics simulations, as it will be discussed in the following section.

Persistence length gives information about the stiffness of the chains and is a parameter that can be extracted from R_c. In charged biopolymers the total persistence length (l) is the sum of the persistence length in the absence (l_o) and presence (l_e) of Coulombic interactions ($l = l_o + l_e$).[29] Electrostatic interactions are mostly screened by the presence of counterions (Na^+) and the chains assume dimensions that correspond to l_o. This length scale can be calculated from the R_c of thin rigid rods as $l_o = \sqrt{12Rc^2}$. Persistence length of ideal random coils is zero whereas for extra-rigid rods approaches infinity. In the samples of the present investigation l_o ranged between ~10-25 Å

revealing particularly flexible chains at all conditions studied (Figure 3, Table S1). It appears that the number of residues consisting l_o are about four at pH 1 and fluctuate from three to six residues at pH 7, as the length of each monomer is between 4.6-5.0 Å depending on their instantaneous conformation (e.g., $^4C_1$, $^1C_4$, etc.). The results demonstrate that multiple factors contribute to the overall persistence length. In the fully protonated state (pH 1) and high temperatures (65 ^oC), DM has no effect on persistence length which remains constant at 15 Å. However, at lower temperatures increasing DM results in a consistent decrease in persistence length. Under neutral conditions (pH 7), a complex relationship between temperature and DM is observed with the greatest changes seen at high temperatures with persistence length reaching a minimum of ~10 Å at DM 70. At low temperatures, a similar pattern emerges but the effect is muted. It should be also noted that the perturbations from 15 Å occur in the same direction as at high temperatures, but with reduced magnitude. These changes occur due to a broad variety of balancing effects including the desolvation energy of non-polar groups (i.e., methyl groups), electrostatic interactions (i.e., carboxyl groups), and excluded volume effects. The temperature dependence of l_o is due to the weakening of intramolecular hydrogen bonding between hydroxyl groups that occurs at higher temperatures resulting in chains with greater flexibility.

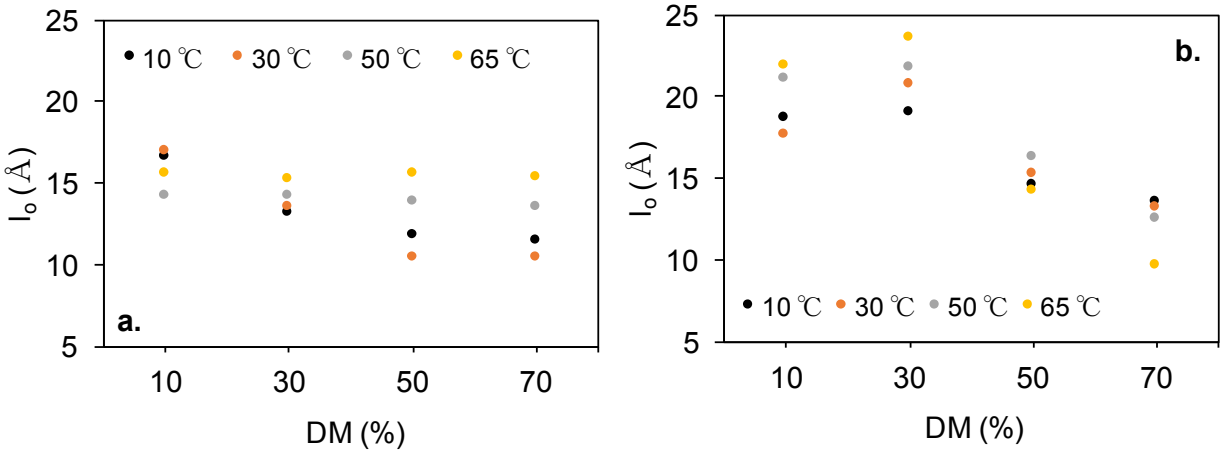

Figure 3: Persistence length of samples as function of temperature and degree of methylesterification in the presence of 100 mM NaCl at: a) pH 1, and b) pH 7.

Dissociation of carboxylic groups at high pH values enhances electrostatic interactions resulting in chain stiffening whereas increase in hydrophobic character of the samples imparts flexibility to the chains. Persistence lengths measurements of pectin depend on the experimental technique and method that is used to calculate it. Consequently, the relative shift in the size with respect to the environmental changes (e.g., structure, pH, salt, etc.) is more informative compared to its absolute value. For instance, persistence lengths of pectin measured with scattering techniques in very similar conditions resulted in l_o varying between 45-75 Å[6] or 38-83 Å[8] and showed responsiveness of conformation to DM, rhamnogalacturonan-I (RG-I) content, and pH, although a clear relationship was not established, as in the present study. Studies of l_o of pectin samples from various botanical sources using intrinsic viscosity and modelling tend to result in somewhat greater values ranging between 70-90 Å, [35] 14-100 Å, [36] or 100-130 Å [9] whereas new methodologies using electrokinetic potential measurements are in good agreement[37] with the results of the present study. Nevertheless, the sensitivity of chain flexibility on degree of methylesterification and rhamnose content has been established in the aforementioned studies showing that RG-I-rich pectins are the most flexible. In addition, molecular dynamics simulations of polygalacturonic acid yielded persistence lengths of 110 Å for protonated chains and 300 Å for deprotonated chains[38] also confirming the loss of flexibility we observed at neutral pH particularly for samples with low DM (Figure 3). It is important to note that chains showed only a marginal preference to stiffer conformations with increase in temperature, however, its influence on persistence length was not conclusive. Taking everything into account, it is inferred that chain flexibility increases with DM and at acidic pH.

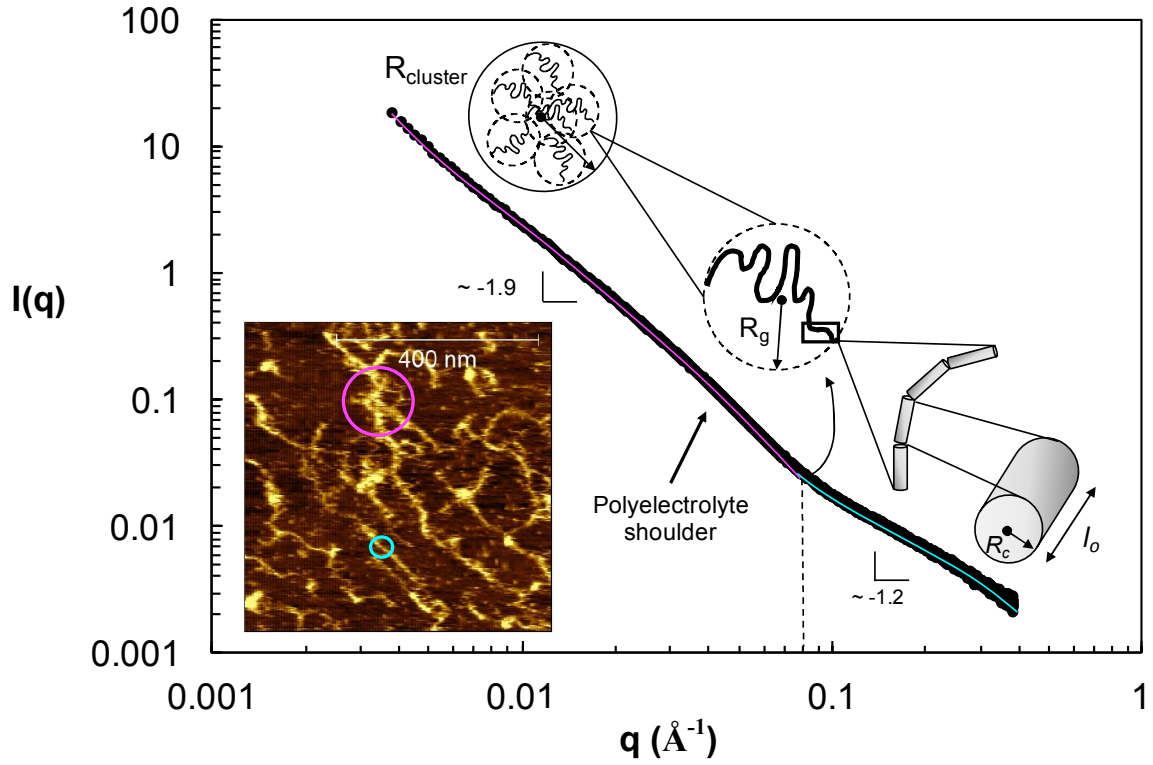

Figure 4: Characteristic Porod plots of pectin samples. The first level of structure ($R_{cluster}$) is associated with the length scale of clusters (large purple circle in AFM). The shoulder in the scattering curve is due to the charges on the polyelectrolyte backbone. The transition to the higher length scales (dashed black line) is associated with the radius of gyration (R_g) of individual pectin chains (small turquoise circle in AFM). Purple (scattering from clusters) and turquoise (scattering of pectin chains) lines show an example of curve fitting using an empirical functional (guide to the eye only). Inset shows atomic force image of sample DM 70. l_o is the persistence length, and R_c the cross-sectional radius of gyration. z-Scale on the AFM image is from 1.27 to 2.56 nm, as the highest (bright yellow) and the lowest (black) points of the scans.

Double logarithmic plots of I(q) vs. q (Porod plots) provide information on the local structure of the biopolymer and give first insights into the solution conformation of the samples (Figure 4). The first level of structure ($q < 0.003$ Å^{-1}), as mentioned previously, is associated with the length scale of the clusters. As SAXS cannot resolve this dimension we employed atomic force microscopy (AFM) for selected samples to obtain structural information at lower length scales. Although AFM gives a snapshot of solution behaviour, as samples dry on the mica before

visualisation, the technique is adequate to provide tangible evidence of clustering. Indeed, chains protrude radially from the centre of the aggregates as rods, branched or kinked chains (Figure 4, inset, and Figure S3). The radius of the aggregated structures was estimated between 100 – 200 nm (1000 – 2000 Å), which should correspond to the order of magnitude of the radius of gyration of the clusters ($R_{cluster}$) (Figure 4). Aggregated structures forming at concentrations above 0.01 mg/mL of high and low methoxylated pectins have previously been observed with AFM.[39, 40] At higher-q a weak shoulder is observed on the curves at about 0.03 Å^{-1}, which was more evident for samples at pH 7 and low DM. This length scale represents the polyelectrolyte peak that either dissipates or merges for most of the samples in the low-q clustering region. This occurs as the presence of salt makes the charged domains larger and shifts the peak to low-q values and the solution exhibits mostly "neutral" polymer behaviour.[26]

Fractal dimensions from the slopes of Porod plots can be obtained to evaluate structure evolution at different conditions. Slopes from low- and high-q regions fluctuate around -1.9 or -1.2, respectively, depending on the conditions (Table S1). A fractal dimension of 2 describes a random walk and indicates that pectin chains will randomly fill the space within the clusters. Self-avoiding random walk that takes into account excluded volume interactions scale with exponent of 1.6 and indicate stiffer chains. A fractal dimension of ~1.9 for the low-q region shows that the arrangement of pectin chains within the clusters is mostly random. The transition to exponent of ~1.2 is related to the scattering of stiff rods[41] and corresponds to the radius of gyration (R_g) of the pectin chains. Depending on conditions, the transition between high- and low-q regions occurred between 0.015-0.1 Å^{-1} with R_g values fluctuating in real space between ~ 63-420 Å (6.3-42 nm). Estimation of R_g from light scattering data (~36 nm) also falls within this range corresponding to the specific conditions of elution (pH 8.6). The transition occurs for most systems at around 0.08 Å^{-1} (black dashed line on Figure 4) representing an R_g of about 78 Å (7.8 nm) and is in very close agreement with the transitions or R_g values observed for apple, [42] citrus,[43] or okra pectin.[8] It should be mentioned, however, that it was difficult to distinguish the exact transition point with

sufficient accuracy for all samples at different conditions and a relationship could not be established.

Even though determination of the R_g was problematic, it was still possible to observe the evolution of the structure as a function of degree of methylesterification, pH, and temperature by following the development of fractal dimensions (Figure 5).

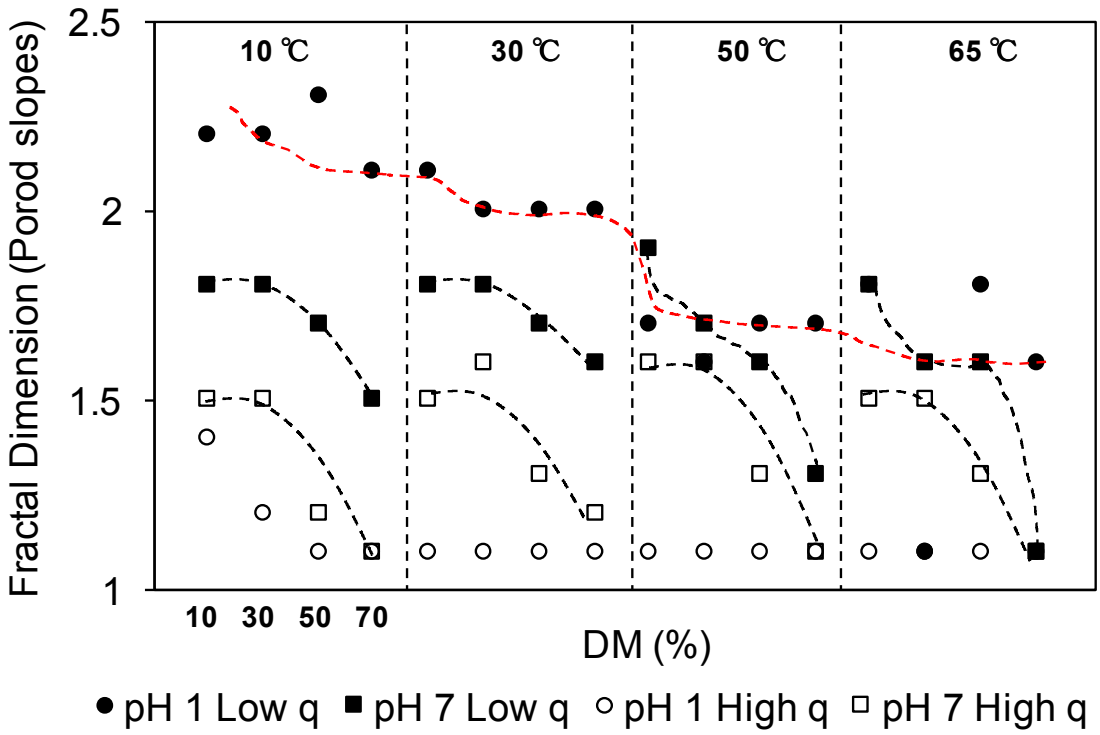

Figure 5: Fractal dimensions (Porod slopes) obtained for samples in the dilute regime. Plot is divided into four regions of increasing temperature (10, 30, 50 or 65 ^{o}C). Within each region from left to right degree of methylesterification increases (10, 30, 50, or 70%). Red dashed line shows a continuous decrease of fractal dimension at pH 1 with temperature. Black dashed lines show that at pH 7 increase of DM results in decrease of fractal dimension.

The low-q slopes that give information on the cluster structure reveal the clear influence of pH as fractal dimensions are higher at pH 1 than pH 7 due to reduction of electrostatic repulsion and closer packing of the chains. Differences in the clustering strength between the two ionisation extremes persist up to 50 ^{o}C (red dashed line). Beyond that temperature, differences in the fractal dimensions between pH 1 and pH 7 become marginal indicating disassembly of the clusters or

chain expansion due to increased thermal energy (Figure 5). It is worth noticing that the high-*q* slope at pH 1 was found to be invariant (~1.1) showing that chains attain stiff rod conformations at all experimental conditions studied. In addition, a clear trend between DM and structure evolution is observed for samples at pH 7, as increase of DM beyond 30% results in substantial decrease of fractal dimension at all temperatures (curved black dashed lines, Figure 5). This shows that packing of chains in samples with high DM is not efficient, perhaps as a result of steric hindrance of the methyl groups. This is in congruence with the increase of hydrodynamic volume observed in intrinsic viscosity measurements (Table 1).

Temperature modulation plays minimal role on the overall shape of the scattering curve for samples of the same concentration, DM and pH (Figure S4a). Generally, low temperatures enhance hydrogen bonding whereas high temperatures hydrophobic interactions. At high temperatures ($T < 50\ ^{o}C$) the low-*q* feature of the curves becomes weaker indicating that hydrogen bonding should be the responsible thermodynamic driving force for cluster formation whereas hydrophobic interactions have negligible influence even for the samples of high DM. Hydrogen-bond induced aggregation has been previously demonstrated with the influence of urea on flow properties of low methoxyl pectin solutions.[44] The total scattering intensity increased with DM, as the electron density difference between the sample and the aqueous environment increases with DM yet the curve shape remained the same (Figure S4b). As the atomic number of carbon is greater than that of hydrogen (-COO-CH_3 *vs.* -COO-H) the overall intensity of scattering curve will inevitably increase demonstrating the importance of the methyl group. This is also illustrated by the influence of pH, as scattering curves of samples with low DM have greater intensity at high pH values as a result of electrostatic repulsion between the chains thus increasing the volume of the particles and the contrast between solvent and solute (Figure S5a). On the contrary, curves of DM 70 overlap at pH 7 and 1 (Figure S5b).

To further characterise the data in the semi dilute region of the biopolymers (10 mg/mL), an empirical functional was fitted to the data of the form (Figure 4, purple and turquoise lines):

$$I(q) = \frac{A}{q^n} + \frac{C}{1 + (q\xi)^m} + b$$

The first term describes the scattering from clusters, and the second term is a Lorentzian function describing scattering from polymer chains.[45] This second term characterizes the polymer-solvent interactions and therefore the thermodynamics of the system. Parameters *A, C*, background *b*, and exponents *n* and *m* were used as fitting parameters with the aim to obtain ξ that is the correlation length of the polymer chains (Table S1). It should be noted that exponents *n* and *m* are equivalent to low-*q* and high-*q* slopes, respectively (Figure 5). Correlation lengths varied dramatically with both pH and DM ranging between 10-50 Å at pH 1 and 20-115 Å at pH 7. In particular, increase of DM resulted in decrease of ξ a trend that was observed at both pH values (Figure 6).

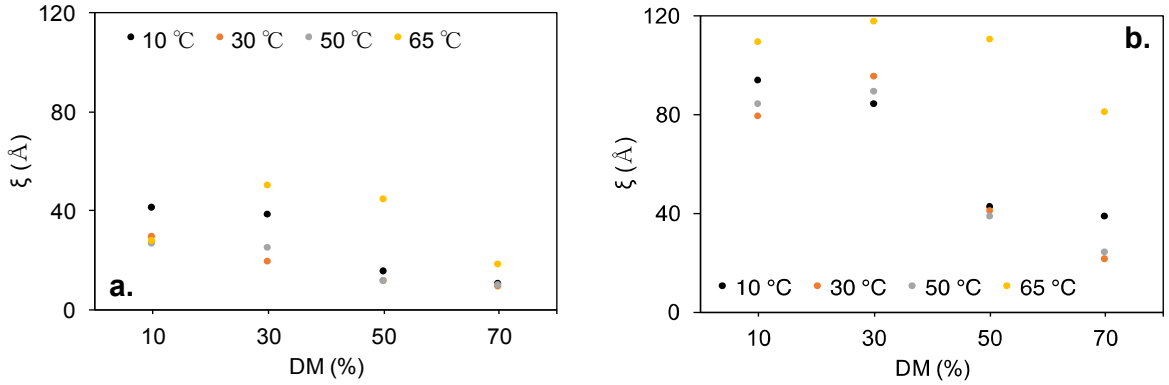

Figure 6: Correlation lengths, ξ, of samples as function of temperature and degree of methylesterification, a) at pH 1, and b) at pH 7.

At distances smaller than ξ, chain segments are surrounded by the solvent or other segments that belong to the same chain whereas at length scales greater than ξ, chains entangle. We should notice that there is an abrupt fall of ξ values for DM > 30 particularly at pH 7.0. Smaller ξ values at low pH indicate that the "correlation blobs" are smaller pointing to more dense structures. In addition to suppression of electrostatic repulsion at low pH, increase of hydrophobic attraction with DM brings the chains together, further decreasing correlation length. The effect is more prominent at neutral pH where increase in electrostatic repulsion almost doubles ξ values.

Correlation length trends are in accordance with those of intrinsic viscosity (Table 1) indicating that high methoxyl pectins would overlap at lower critical concentrations (c^*) than their counterparts with low DM, as polymers with high [η] usually exhibit lower c^*. [46] This has been also clearly demonstrated with okra pectin where samples with higher DM at pH 7 showed higher c^* values.[47] Finally, temperature does not seem to have a clear influence on correlation length although at the highest temperature studied ξ seems to depart from the overall behaviour.

3.3 Molecular dynamics

Molecular dynamics modelling was performed in explicit solvent to assess the conformational behaviour of pectin at boundary environmental conditions. It should be noted that the decamer that has been modelled is essentially polygalacturonic acid oligomer with variable degree of methylesterification while rhamnose residues that impart conformational flexibility[35] have been neglected.

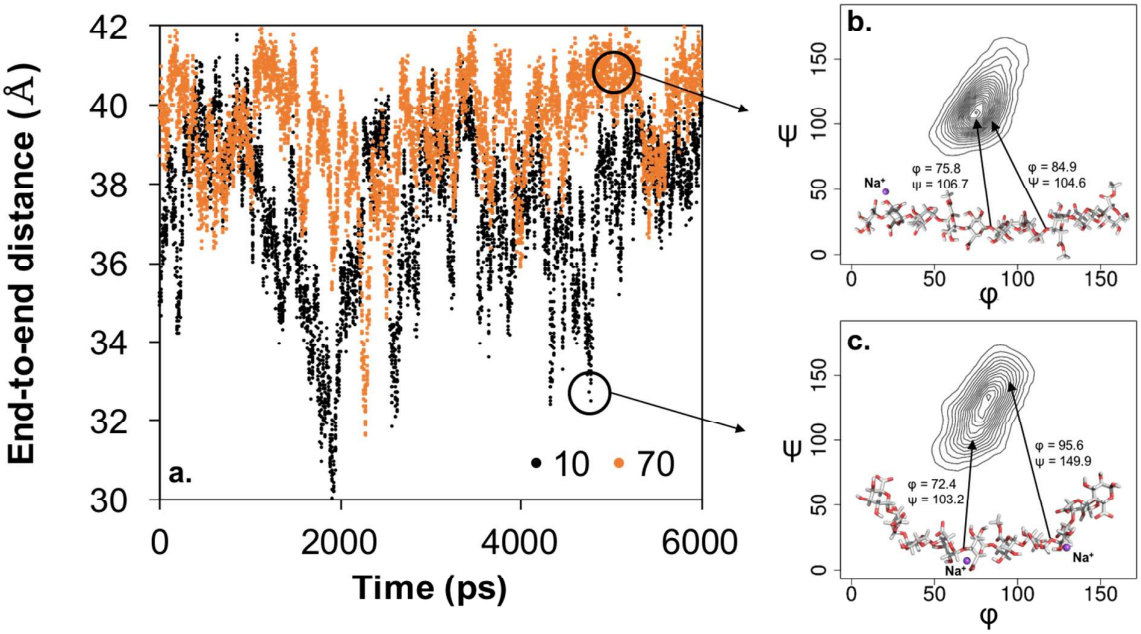

Figure 7: (a) End-to-end distances of decamer systems at pH 7 with 10% and 70% methylesterification over the last 6 ns of MD simulations in explicit solvent. Contour plots showing the population of torsion angles over the same time scale with (b) 70% methylesterification, and (c) 10% methylesterification both at pH 7. Insets show representative

decamer structures from extended (b) and bended (c) conformations. Sodium counterions are shown as purple spheres.

It should be mentioned that to draw quantitative comparisons it would require much longer simulation times so as to observe reorientation of glycosidic linkages (~50-100 ns) or ring flips (~1 μs). Nevertheless, the simulation time we have used (10 ns) is comparable to previous MD studies of carbohydrate 10-mers[48] or 25-mers[3] and is suitable to give first insights on the dependency of local conformations on sodium, degree of methylesterification, and pH. In addition, the findings of the simulations remain in qualitative agreement with the experimental findings, as is discussed below. Chain conformations depend on the torsion angles (φ, ψ) and can be visualised by contour plots of occupancy (Figure 7 and Figure S6). Torsion angles (φ, ψ) of pectin decamers at the four extremes of conformational behaviour revealed a single high-occupancy region centred around $\varphi = 70^{o}$ and $\psi = 100^{o}$ for all systems in agreement with potential energy maps previously reported for dimers of D-GalA.[38, 49] Systems representing decamers with 10% and 70% DM at pH 1 did not show any systematic differences in both torsion angles and end-to-end distances (Figure S6). The charge densities are equal between the two systems and chain lengths are the same, revealing very little influence of methyl substitution at low pH values. The conformational landscape, however, changes once the pH is raised to neutral. As Na^{+} and Cl^{-} ions were included in the explicit solvent simulations, transient but frequent interactions between sodium and pectin can be observed (Figure 7). These electrostatic interactions predominantly involve the carboxylic acid group of galacturonic acid, effectively screening the electrostatic repulsion, but may also involve divalent interactions with oxygen atoms of neighbouring residues (e.g., OH on C2). At pH 7, and low DM the greater charge density facilitates the interaction of sodium ions with adjacent pectin residues. This alters significantly the conformational landscape, widening the distribution of torsion angles (Figure 7). Consequently, it causes chain bending due to counterion condensation thus allowing them to adopt a more coiled conformation, which is also reflected in the end-to-end distances of the oligomer (Figure 7). This provides a plausible mechanism to

explain the lower fractal dimension of DM70 (extended chains) compared to DM10 (bended chains) at neutral pH (open squares, Figure 5). Such bending has been also previously reported for poly-galacturonic acid oligomers [38] although the influence of degree of methylesterification was not examined. At pH 1, in the absence of these counterion interactions, the decamer predominantly occupies a highly extended conformation irrespective of the degree of methylesterification (Figure S6), which is consistent with the limited differences in fractal dimensions observed at pH 1 (open circles, Figure 5). It should be mentioned that counterion condensation effects depend on the force-field-inherent ability to predict either the "loose" or the "tight" ion binding and Lennard-Jones parameters may require optimisation to accurately reproduce experimental data.[50] Despite that fact, the observations of end-to-end distance behaviour in molecular dynamics are in qualitative agreement with Kratky plots at pH 1 and 7 (Figure 2b) obtained from experimental data where, as previously discussed, samples with low degree of methylesterification tend to be more coiled at pH 7. In addition, the pH-dependent alteration in the conformations of the glycosidic linkage is also in qualitative agreement with simulations of the conformation of protonated, deprotonated and esterified uronate residues obtained using different force field.[51] Finally, besides the local interactions between adjacent residues, counterion condensation may also facilitate the interaction between pectin chains.

4. Conclusions

The influence of degree of methylesterification, pH, temperature, concentration in the presence of salt on the macromolecular interactions of pectin in solution has been explored. Irrespectively of the experimental conditions, two levels of structure have been observed; one that is associated with radius of gyration of clusters (~100-200 nm) and a second with the radius of gyration of single chains (~6-42 nm). Hydrogen bonding was found to be the responsible thermodynamic driving force for cluster formation. LM-pectins at pH 7 attain bended conformations due to counterion condensation but gradually expand with increase of the degree of methylesterification, as a result of decreased charge density. Chain flexibility generally increases

with DM and at acidic pH values where galacturonic acid residues are fully protonated. Overall, HM-pectins create structures of lower fractal dimension resulting in less efficient packing of the chains in contrast to their LM counterparts. The present work unveiled the solution conformation of pectin covering most of its industrially and biologically relevant environments thus enabling rational design of advanced biomaterials based on pectin.

Acknowledgements

We are grateful to the Diamond Light Source for the beam time award (ref: SM17074) on beamline B21. We are also thanking Dr. Robert Rambo and Dr. Katsuaki Inoue for their assistance during the experimental work and help with the analysis of some of the SAXS results. P Gunning and P Wilde gratefully acknowledge the BBSRC for supporting the work through the Food and Health Institute Strategic Programme Grant.

Supporting Information Paragraph

Table S1: Molecular characteristics of pectin samples obtained from SAXS data analysis. χ^2/N is an index of goodness of fitting with values close to zero indicating perfect fitting and values below 100 are generally deemed as acceptable. *Rc* is the cross-sectional radius of gyration, l_o is the persistence length and, ξ is the correlation length. **Figure S1**: Concentration dependence of scattering intensity curves of pectin samples. **Figure S2**: Typical Kratky plots of salt free pectin samples with different DM at pH 7. The counterion condensation peak is not observed. **Figure S3**: Typical AFM images of pectin with: a) DM 10 and b) DM 70. **Figure S4**: Representative scattering curves of pectin samples showing: a) the effect of temperature, and b) the effect of degree of degree of methylesterification. Low-*q* scattering intensity decreases with temperature indicating that hydrogen bonds play important role in clustering. Scattering intensity increase with degree of methylesterification as a result of additional $-CH_3$ groups on the chains. **Figure S5:** pH-dependence of pectin samples with a) DM 10 and b) DM 70. The difference in the scattering intensity between pH values is eliminated with increase of DM. **Figure S6**: (a, c, e) Conformational landscapes of pectin decamers simulated by MD at pH 1, and (b, d, f) at pH 7. Contour plots showing the population of torsion angles over 6 ns of MD simulation with (a, b) DM 70%, and (c, d) DM 10%. End-to-end distances of decamer systems with 10% and 70% methylesterification at (e) pH 1 and (f) pH 7 over the same time scale.

5. References

1. Rinaudo, M. Polyelectrolyte Properties of a Plant and Animal Polysaccharide. *Struct. Chem.* **2009,** *20*, 277-289
2. Djabourov, M.; Nishinari, K.; Ross-Murphy, S. B. *Physical Gels from Biological and Synthetic Polymers*; Cambridge University Press: Cambridge, 2013.
3. Irani, A. H.; Owen, J. L.; Mercadante, D.; Williams, M. A. K. Molecular Dynamics Simulations Illuminate the Role of Counterion Condensation in the Electrophoretic Transport of Homogalacturonans. *Biomacromolecules* **2017,** *18*, 505-516
4. Mohnen, D. Pectin Structure and Biosynthesis. *Curr. Opin. Plant Biol.* **2008,** *11*, 266-277
5. Daas, P. J. H.; Meyer-Hansen, K.; Schols, H. A.; De Ruiter, G. A.; Voragen, A. G. J. Investigation of the Non-Esterified Galacturonic Acid Distribution in Pectin with Endopolygalacturonase. *Carbohydr. Res.* **1999,** *318*, 135-145
6. Cros, S.; Garnier, C.; Axelos, M. A. V.; Imberty, A.; Perez, S. Solution Conformations of Pectin Polysaccharides: Determination of Chain Characteristics by Small Angle Neutron Scattering, Viscometry, and Molecular Modeling. *Biopolymers* **1996,** *39*, 339-352
7. Ralet, M.-C.; Crepeau, M.-J.; Lefebvre, J.; Mouille, G.; Hofte, H.; Thibault, J.-F. Reduced Number of Homogalacturonan Domains in Pectins of an Arabidopsis Mutant Enhances the Flexibility of the Polymer. *Biomacromolecules* **2008,** *9*, 1454-1460
8. Alba, K.; Bingham, R. J.; Kontogiorgos, V. Mesoscopic Structure of Pectin in Solution. *Biopolymers* **2017,** *107*, 1-8
9. Morris, G. A.; de al Torre, J. G.; Ortega, A.; Castile, J.; Smith, A.; Harding, S. E. Molecular Flexibility of Citrus Pectins by Combined Sedimentation and Viscosity Analysis. *Food Hydrocolloids* **2008,** *22*, 1435-1442
10. Huggins, M. L. The Viscosity of Dilute Solutions of Long-Chain Molecules. Iv. Dependence on Concentration. *J. Am. Chem. Soc.* **1942,** *64*, 2716-2718
11. Chatjigakis, A. K.; Pappas, C.; N.Proxenia; O.Kalantzi; P.Rodis; Polissiou, M. Ft-Ir Spectroscopic Determination of the Degree of Esterification of Cell Wall Pectins from Stored Peaches and Correlation to Textural Changes. *Carbohydr. Polym.* **1998,** *37*, 395-408
12. Bradford, M. M. A Rapid and Sensitive Method for the Quantitation of Microgram Quantities of Protein Utilizing the Principle of Protein-Dye Binding. *Anal. Biochem.* **1976,** *72*, 248-254
13. Filik, J.; Ashton, A. W.; Chang, P. C. Y.; Chater, P. A.; Day, S. J.; Drakopoulos, M.; Gerring, M. W.; Hart, M. L.; Magdysyuk, O. V.; Michalik, S.*, et al.* Processing Two-Dimensional X-Ray Diffraction and Small-Angle Scattering Data in Dawn 2. *J. Appl. Crystallogr.* **2017,** *50*, 959-966
14. Case, D. A.; Cerutti, D. S.; Cheatham, I., T.E. ; Darden, T. A.; Duke, R. E.; Giese, T. J.; Gohlke, H.; Goetz, A. W.; Greene, D.; Homeyer, N.*, et al. Amber 17*, University of California: San Fransisco, 2017.
15. Kirschner, K. N.; Yongye, A. B.; Tschampel, S. M.; González-Outeiriño, J.; Daniels, C. R.; Foley, B. L.; Woods, R. J. Glycam06: A Generalizable Biomolecular Force Field. Carbohydrates. *J. Comput. Chem.* **2008,** *29*, 622-655
16. Roe, D. R.; Cheatham, T. E. Ptraj and Cpptraj: Software for Processing and Analysis of Molecular Dynamics Trajectory Data. *J. Chem. Theory Comput.* **2013,** *9*, 3084-3095
17. Team, R. C. *R: A Language and Environment for Statistical Computing.* , R Foundation for Statistical Computing: Vienna, Austria, 2013.
18. Humphrey, W.; Dalke, A.; Schulten, K. Vmd: Visual Molecular Dynamics. *J. Mol. Graphics* **1996,** *14*, 33-38
19. Schrodinger, LLC, The Pymol Molecular Graphics System, Version 1.8. 2015.
20. Williams, M. A. K.; Foster, T. J.; Schols, H. A. Elucidation of Pectin Methylester Distributions by Capillary Electrophoresis. *J. Agric. Food. Chem.* **2003,** *51*, 1777-1781
21. Guillotin, S. E.; Bakx, E. J.; Boulenguer, P.; Mazoyer, J.; Schols, H. A.; Voragen, A. G. J. Populations Having Different Gala Blocks Characteristics Are Present in Commercial Pectins

Which Are Chemically Similar but Have Different Functionalities. *Carbohydr. Polym.* **2005,** *60*, 391-398
22. Dobrynin, A. V.; Colby, R. H.; Rubinstein, M. Scaling Theory of Polyelectrolyte Solutions. *Macromolecules* **1995,** *28*, 1859-1871
23. Stokke, B. T.; Draget, K. I.; Smidsrød, O.; Yuguchi, Y.; Urakawa, H.; Kajiwara, K. Small-Angle X-Ray Scattering and Rheological Characterization of Alginate Gels. 1. Ca-Alginate Gels. *Macromolecules* **2000,** *33*, 1853-1863
24. Denef, B.; Mischenko, N.; Koch, M. H. J.; Reynaers, H. Small-Angle X-Ray Scattering of K- and I-Carrageenan in Aqueous and in Salt Solutions. *Int. J. Biol. Macromol.* **1996,** *18*, 151-159
25. Khan, S.; Birch, J.; Harris, P.; Van Calsteren, M.-R.; Ipsen, R.; Peters, G. H. J.; Svensson, B.; Almdal, K. Revealing the Compact Structure of Lactic Acid Bacterial Heteroexopolysaccharides by Saxs and Dls. *Biomacromolecules* **2017,** *18*, 747-756
26. Horkay, F.; Hammouda, B. Small-Angle Neutron Scattering from Typical Synthetic and Biopolymer Solutions. *Colloid. Polym. Sci.* **2008,** *286*, 611-620
27. Nagvekar, M.; Tihminlioglu, F.; Danner, R. P. Colligative Properties of Polyelectrolyte Solutions. *Fluid Phase Equilib.* **1998,** *145*, 15-41
28. Manning, G. S. Limiting Laws and Counterion Condensation in Polyelectrolyte Solutions I. Colligative Properties. *J. Chem. Phys.* **1969,** *51*, 924-933
29. Dobrynin, A. V.; Rubinstein, M. Theory of Polyelectrolytes in Solutions and at Surfaces. *Prog. Polym. Sci.* **2005,** *30*, 1049-1118
30. Thibault, J. F.; Rinaudo, M. Interactions of Mono- and Divalent Counterions with Alkali- and Enzyme-Deesterified Pectins in Salt-Free Solutions. *Biopolymers* **1985,** *24*, 2131-2143
31. Murnen, H. K.; Rosales, A. M.; Dobrynin, A. V.; Zuckermann, R. N.; Segalman, R. A. Persistence Length of Polyelectrolytes with Precisely Located Charges. *Soft Matter* **2013,** *9*, 90-98
32. Qu, D.; Pedersen, J. S.; Garnier, S.; Laschewsky, A.; Möhwald, H.; Klitzing, R. v. Effect of Polymer Charge and Geometrical Confinement on Ion Distribution and the Structuring in Semidilute Polyelectrolyte Solutions: Comparison between Afm and Saxs. *Macromolecules* **2006,** *39*, 7364-7371
33. Chremos, A.; Douglas, J. F. Counter-Ion Distribution around Flexible Polyelectrolytes Having Different Molecular Architecture. *Soft Matter* **2016,** *12*, 2932-2941
34. Carrillo, J.-M. Y.; Dobrynin, A. V. Polyelectrolytes in Salt Solutions: Molecular Dynamics Simulations. *Macromolecules* **2011,** *44*, 5798-5816
35. Axelos, M. A. V.; Thibault, J. F. Influence of the Substituents of the Carboxyl Groups and of the Rhamnose Content on the Solution Properties and Flexibility of Pectins. *Int. J. Biol. Macromol.* **1991,** *13*, 77-82
36. Morris, G. A.; Ralet, M.-C.; Bonnin, E.; Thibault, J.-F. ß.; Harding, S. E. Physical Characterisation of the Rhamnogalacturonan and Homogalacturonan Fractions of Sugar Beet (Beta Vulgaris) Pectin. *Carbohydr. Polym.* **2010,** *82*, 1161-1167
37. Abodinar, A.; Smith, A. M.; Morris, G. A. A Novel Method to Estimate the Stiffness of Carbohydrate Polyelectrolyte Polymers Based on the Ionic Strength Dependence of Zeta Potential. *Carbohydr. Polym.* **2014,** *112*, 6-9
38. Noto, R.; Martorana, V.; Bulone, D.; San Biagio, P. L. Role of Charges and Solvent on the Conformational Properties of Poly(Galacturonic Acid) Chains: A Molecular Dynamics Study. *Biomacromolecules* **2005,** *6*, 2555-2562
39. Fishman, M. L.; Cooke, P. H.; Chau, H. K.; Coffin, D. R.; Hotchkiss Jr, A. T. Global Structures of High Methoxyl Pectin from Solution and in Gels. *Biomacromolecules* **2007,** *8*, 573-578
40. Fishman, M. L.; Chau, H. K.; Qi, P. X.; Hotchkiss, A. T.; Garcia, R. A.; Cooke, P. H. Characterization of the Global Structure of Low Methoxyl Pectin in Solution. *Food Hydrocolloids* **2015,** *46*, 153-159
41. Beaucage, G. Small-Angle Scattering from Polymeric Mass Fractals of Arbitrary Mass-Fractal Dimension. *J. Appl. Crystallogr.* **1996,** *29*, 134-146

42. Mansel, B. W.; Chu, C.-Y.; Leis, A.; Hemar, Y.; Chen, H.-L.; Lundin, L.; Williams, M. A. K. Zooming In: Structural Investigations of Rheologically Characterized Hydrogen-Bonded Low-Methoxyl Pectin Networks. *Biomacromolecules* **2015,** *16*, 3209-3216
43. Fishman, M. L.; Pfeffer, P. E.; Barford, R. A.; Doner, L. W. Studies of Pectin Solution Properties by High-Performance Size Exclusion Chromatography. *J. Agric. Food. Chem.* **1984,** *32*, 372-378
44. Li, X.; Al-Assaf, S.; Fang, Y.; Phillips, G. O. Characterisation of Commercial Lm-Pectin in Aqueous Solution. *Carbohydr. Polym.* **2013,** *92*, 1133-1142
45. Hammouda, B.; Ho, D. L.; Kline, S. Insight into Clustering in Poly(Ethylene Oxide) Solutions. *Macromolecules* **2004,** *37*, 6932-6937
46. Sperling, L. H. *Introduction to Physical Polymer Science*; John Willet & Sons, Inc.: New Jersey, 2006.
47. Alba, K.; Laws, A. P.; Kontogiorgos, V. Isolation and Characterisation of Acetylated Lm-Pectins Extracted from Okra Pods. *Food Hydrocoilloids* **2015,** *43*, 726-735
48. Verli, H.; Guimarães, J. A. Molecular Dynamics Simulation of a Decasaccharide Fragment of Heparin in Aqueous Solution. *Carbohydr. Res.* **2004,** *339*, 281-290
49. Braccini, I.; Grasso, R. P.; Pérez, S. Conformational and Configurational Features of Acidic Polysaccharides and Their Interactions with Calcium Ions: A Molecular Modeling Investigation. *Carbohydr. Res.* **1999,** *317*, 119-130
50. Project, E.; Nachliel, E.; Gutman, M. Parameterization of Ca+2–Protein Interactions for Molecular Dynamics Simulations. *J. Comput. Chem.* **2007,** *29*, 1163-1169
51. Panczyk, K.; Gaweda, K.; Drach, M.; Plazinski, W. Extension of the Gromos 56a6carbo/Carbo_R Force Field for Charged, Protonated, and Esterified Uronates. *The Journal of Physical Chemistry B* **2018,** *122*, 3696-3710

TOC Graphic

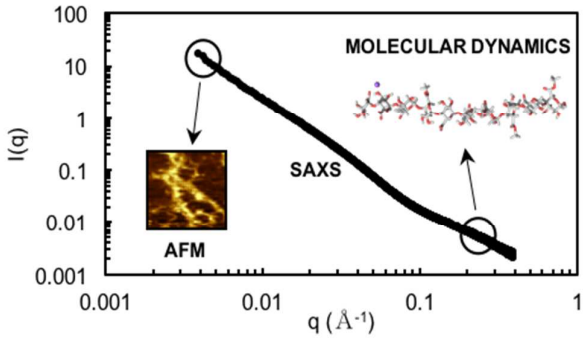
MOLECULAR DYNAMICS
SAXS
AFM
I(q)
q (Å-1)
100
10
1
0.1
0.01
0.001
0.001
0.01
0.1
1